International Journal of Heat and Mass Transfer 52 (2009) 2273–2288

Contents lists available at ScienceDirect

International Journal of Heat and Mass Transfer

journal homepage: www.elsevier.com/locate/ijhmt

# Ammonia two-phase flow in a horizontal smooth tube: Flow pattern observations, diabatic and adiabatic frictional pressure drops and assessment of prediction methods

Ricardo J. da Silva Lima [a,*], Jesús Moreno Quibén [a], Cornel Kuhn [a,b], Tahsin Boyman [b], John R. Thome [a]

[a] Laboratoire de Transfert de Chaleur (LTCM), Sciences et Techniques de l'Ingénieur (STI), École Polytechnique Fédérale de Lausanne (EPFL), Station 9, CH-1015 Lausanne, Switzerland
[b] Hochschule Luzern – Technik & Architektur (former HTA), Technikumstrasse 21, CH-6048 Horw, Switzerland

ARTICLE INFO

*Article history:*
Received 8 October 2008
Available online 29 January 2009

*Keywords:*
Ammonia
R717
Experimental
Flow boiling
Flow pattern observations
Diabatic
Adiabatic
Two-phase frictional pressure drop
Comparisons
Prediction methods

ABSTRACT

The present study illustrates new experimental two-phase flow pattern observations together with diabatic boiling and adiabatic two-phase frictional pressure drop results for ammonia (R717) flowing inside a 14-mm internal diameter, smooth horizontal stainless steel tube. The flow pattern observations were made for mass velocities of 50, 100 and 160 kg $s^{-1}$ $m^{-2}$ and saturation temperatures of −14, −2 and 12 °C for vapor qualities ranging from 0.05 to 0.6. The flow patterns observed during the study included: *stratified-wavy*, *slug-stratified-wavy*, *slug*, *intermittent* and *annular*. For all the experimental conditions, the flow structure observations were compared against the predictions of the flow pattern map model of Wojtan et al. [L. Wojtan, T. Ursenbacher, J.R. Thome, Investigation of flow boiling in horizontal tubes: part I – a new diabatic two-phase flow pattern map, Int. J. Heat Mass Transfer 48 (2005) 2955–2969] and showed very good correspondence. The frictional pressure drop measurements were obtained for vapor qualities from 0.05 to 0.6, saturation temperatures from −14 to 14 °C, mass velocities from 50 to 160 kg $s^{-1}$ $m^{-2}$ and heat fluxes from 12 to 25 kW $m^{-2}$. The experimental results show the traditional pressure drop trends: the frictional pressure drop increases with vapor quality and mass velocity. Moreover, the results also show that both diabatic and adiabatic frictional pressure drop values are similar, that is, the boiling process in itself does not affect the frictional pressure drop. The correlations of Friedel [L. Friedel, Improved friction drop correlations for horizontal and vertical two-phase pipe flow, in: European Two-Phase Flow Group Meeting, paper E2, Ispra, Italy, 1979], Lockhart and Martinelli [R.W. Lockhart, R.C. Martinelli, Proposed correlation of data for isothermal two-phase two-component in pipes, Chem. Eng. Process 45 (1949) 39–48] and Müller-Steinhagen and Heck [H. Müller-Steinhagen, K. Heck, A simple friction pressure correlation for two-phase flow in pipes, Chem. Eng. Process 20 (1986) 297–308] predicted only 54%, 52% and 60% of the experimental data within ±30%, respectively. The correlation of Grönnerud [R. Grönnerud, Investigation of liquid hold-up, flow-resistance and heat transfer in circulation type of evaporators, part iv: two-phase flow resistance in boiling refrigerans, in: Annexe 1972-1, Bull. de l'Inst. Froid, 1979] predicted 93% of the data and the flow pattern based method of Moreno Quibén and Thome [J. Moreno Quibén, J.R. Thome, Flow pattern based two-phase frictional pressure drop model for horizontal tubes. Part II: new phenomenological model, Int. J. Heat Fluid Flow 28 (2007) 1060–1072] predicted more than 97% of the experimental data within the same error band, while the latter method captures almost 89% of the data within ±20%.



## 1. Introduction

Although ammonia (R717) has been successfully used in industrial refrigeration plants for over 130 years [7], its use decreased in the last decades in favor of halocarbon refrigerants. Due to the environmental issues such as ozone depletion and global warming, natural working fluids and their use in air-conditioning, heat pump and refrigeration systems are attracting increasing interest from manufacturers, end-users and scientific research. Ammonia is one of those natural refrigerants that recently have been studied to replace CFCs, HCFCs and HFCs in such heat transfer systems. Indeed, ammonia has no ozone depletion potential and a negligible direct global warming potential.

The correct use of ammonia in such systems requires accurate predictive methods for both heat transfer and pressure drop. To

* Corresponding author. Tel.: +41 21 693 59 83; fax: +41 21 693 59 60.
*E-mail addresses:* ricardo.lima@epfl.ch (R.J. da Silva Lima), jmoreno@wolverine.com.pt (J. Moreno Quibén), kirby@mymail.ch (C. Kuhn), tahsin.boyman@hslu.ch (T. Boyman), john.thome@epfl.ch (J.R. Thome).

0017-9310/$ - see front matter © 2008 Elsevier Ltd. All rights reserved.
doi:10.1016/j.ijheatmasstransfer.2008.12.001

**Nomenclature**

*Latin*

| | |
|---|---|
| $c_p$ | specific heat (J kg$^{-1}$ K$^{-1}$) |
| $d$ | diameter (internal) (m) |
| $f$ | friction factor (–) |
| $Fr$ | Froud number (–) |
| $G$ | mass velocity (kg s$^{-1}$ m$^{-2}$) |
| $h$ | enthalpy (J kg$^{-1}$) |
| $L$ | length (m) |
| $m$ | mass flow rate (kg s$^{-1}$) |
| $n$ | number of data points (–) |
| $p$ | pressure (Pa) |
| $q$ | heat flux (W m$^{-2}$) |
| $Q$ | heat power (W) |
| $Re$ | Reynolds number (–) |
| $T$ | temperature (K) or (°C) |
| $We$ | Webber number (–) |
| $X$ | Martinelli parameter (–) |
| $x$ | vapor quality (–) |
| $z$ | axial coordinate (m) |

*Greek*

| | |
|---|---|
| $\varepsilon$ | void fraction (–) or error (%) |
| $\bar{\varepsilon}$ | mean error (%) |
| $\lvert\bar{\varepsilon}\rvert$ | absolute mean error (%) |
| $\rho$ | density (kg m$^{-3}$) |
| $\sigma$ | surface tension (N m$^{-1}$) or standard deviation (%) |
| $\mu$ | viscosity |

*Subscripts*

| | |
|---|---|
| *exp* | experimental |
| *G* | vapor |
| *H* | homogeneous |
| *L* | liquid |
| *ref* | refrigerant |
| *tt* | turbulent liquid and vapor |
| 0 | single-phase, vapor or liquid |

obtain the desired level of accuracy, these methods must be based on an accurate database covering a wide range of experimental conditions. In particular, these databases should include flow pattern information, as the geometrical structure of the flow identifies the distribution of the liquid and vapor phases, and thus, their influence on the heat transfer and pressure drop. Although many methods for heat transfer and pressure drop have been developed empirically without including flow pattern information, it is clear that the accuracy of flow pattern based methods is generally improved in comparison to such methods. The importance of flow patterns as a starting point for the calculation of heat and mass transfer, pressure drop and void fraction was first recognized by Baker [8] in 1954 as established by Kattan et al. [9]. More recently, Silva Lima et al. [10] compared their experimental heat transfer data obtained with R134a to several types of correlations (strictly empirical, strictly convective, superposition and flow pattern based). They concluded that the flow pattern based method predicts most accurately their experimental data and flow pattern transitions could explain the change in trends in heat transfer data quite well.

Heat transfer coefficients and pressure drops are closely related to the local flow structure of the fluid, and thus two-phase flow pattern prediction is an important aspect of modeling evaporation and condensation. Analogous to predicting the transition from laminar to turbulent flow in single-phase flows, two-phase flow pattern maps are used for predicting the transition from one type of two-phase flow pattern to another. Hence, in order to improve local flow pattern based models, a reliable flow pattern map to identify what type of flow pattern exists at the local flow conditions is needed.

Recently, Thome et al. [11] concluded from an extensive literature review on ammonia flow boiling that databases in the literature should be improved in terms of both accuracy and range of experimental conditions. Indeed, only a few studies (such as those of Shah [12–14]; Kabelac and De Buhr [15], Zürcher et al. [16]) have reported flow visualization with ammonia, and even fewer (such as those of Shah [12,14]; Kabelac and De Buhr [15]) have reported experimental pressure drop data for ammonia flow boiling in horizontal smooth tubes. To overcome this paucity of experimental data, a consortium between EPFL and HTA was created in the scope of the European project EFROST (Efficient Refrigerated Food Storage) to study heat transfer and pressure drop of ammonia flow boiling.

Despite the fact that both Shah [12,14] and Kabelac and De Buhr [15] covered a wide range of mass velocities and heat fluxes conditions, each for one internal diameter, their saturation temperatures were restricted to primarily subzero values as shown in Table 1. This study extends these previous studies in terms of saturation temperature conditions into higher values for a new internal diameter as noted in Table 1.

## 2. Flow boiling facility, test section, data reduction and test procedures

### 2.1. Flow boiling facility

Fig. 1 depicts the flow circuit schematic of the ammonia test facility. This facility works on the principle of a single-stage vapor compression cycle. The ammonia vapor leaves the liquid separator and goes into a standard reciprocating compressor. Then, the compressed vapor enters an overdimensioned oil separator to make it oil-free. Both liquid and oil separators on the suction and discharge side, respectively, are vessels big enough to damp possible pulsations from compressor. Afterwards, the vapor flows through a condenser (plate heat exchanger) before entering a subcooler, and then through the Corriolis flow meter. The liquid ammonia then passes through a precooler before being expanded in one of the expansion valves (manually controlled). A preheater allows the vapor quality of the ammonia flow to be set before it enters the test section. All refrigerant flow piping on the facility is well insulated. All the tube connections have a smooth interface in order not to disturb the two-phase flow patterns.

The precooler is a double pipe counter-current flow heat exchanger of 6 m ($2 \times 3$m) length with a cooling capacity of 3 kW. The water–glycol mixture flowing in its outer annulus is cooled in an independent R404A refrigeration plant. Similar to the precooler, the preheater is also a double pipe counter-current flow heat exchanger of 4 m ($2 \times 2$ m) length with a heating capacity of 12 kW. The water–glycol mixture flowing in its outer tube is heated in an independent electrical resistance heater system.

The evaporator is a double pipe counter-current flow heat exchanger, shown in Fig. 2, that consists of two sections with 12 m long. Each section is a serpentine with horizontal straight tube sections of 2 m (plain stainless steel tube with 14 mm ID) connected with U-bends with the same internal diameter. Water–glycol is fed in the concentric outer tube. At the outlet of the preheater and at the inlet/outlet of the U-bends there are straight horizontal tubular sight glasses with the same internal

**Table 1**
Comparison between experimental conditions for frictional pressure drop studies of Shah [12,14], Kabelac and De Buhr [15] and current study.

| Parameter | Shah [12,14] | Kabelac and De Buhr [15] | This study |
|---|---|---|---|
| Refrigerant | Ammonia (R717) | | |
| Tube material | Stainless steel (smooth) | | |
| Orientation | Horizontal | | |
| Internal diameter, $d$ (mm) | 26.2 | 10 | 14 |
| Vapor quality, $x$ (–) | 0.1–0.6 | 0.1–0.6 | 0.1–0.6 |
| Saturation temperature, $T$ (°C) | −15 to 0 | −40 to 4 | −14 to 14 |
| Mass velocity, $G$ (kg s$^{-1}$ m$^{-2}$) | 40–1500 | 50–150 | 55–160 |
| Heat flux, $q$ (kW m$^{-2}$) | 1.6–2.8 | 12–75 | 12–25 |
| Heating medium | Electrical | Condensing ammonia | Hot water–glycol mixture |

diameter as the evaporator tubes for the observation of the flow patterns. Observations presented in this study were made at two locations: at the outlet of the preheater and upstream the U-bends. The experimental parameters – vapor quality, saturation temperature, mass velocity and heat flux – are manually controlled.

### 2.2. Test section

Fig. 3 depicts the two-phase horizontal test setup for measuring the pressure drop, composed of two test sections: one diabatic and one adiabatic. The diabatic section is composed of two coaxial tubes forming an annulus. The refrigerant flows inside the internal stainless steel tube (ID 14 mm) and the hot water–glycol mixture flows in a counterflow direction in the annulus of the double pipe. The diabatic and adiabatic tube lengths are 2115 and 403 mm, respectively. In the diagram, $T$ refers to temperature, $P$ to absolute pressure, $DP$ to differential pressure, $W$ to water, $R$ to refrigerant, $V$ to a bypass valve and the numbers refer to the different sensors. Table 2 shows the axial position and number of thermocouples at each measurement section.

### 2.3. Calibration, experimental procedure and data acquisition

The calibration of the thermocouples was made *in situ*, using two PTC100 thermometers placed in the hot water–glycol side of the test section (annulus). The temperature measurements were made at steady, adiabatic conditions over a temperature range of −20 to 15 °C for both positive and negative changes of temperature of the water–glycol mixture. The accuracy of the thermocouples was found to be ±0.03 °C.

Two different types of pressure transducers were used in this study. A pair of absolute pressure transducers, to determine the saturation temperature ranged 1–25 bar. They were calibrated with a very accurate balance and their accuracy was found to be ±20 mbar within the pressure range of the tests. Two differential pressure transducers were used for the pressure drop. An accuracy of ±0.075% FS was given by the supplier. After inhouse calibration against a water column, this value was found to be realistic and taken as the accuracy of the transducers.

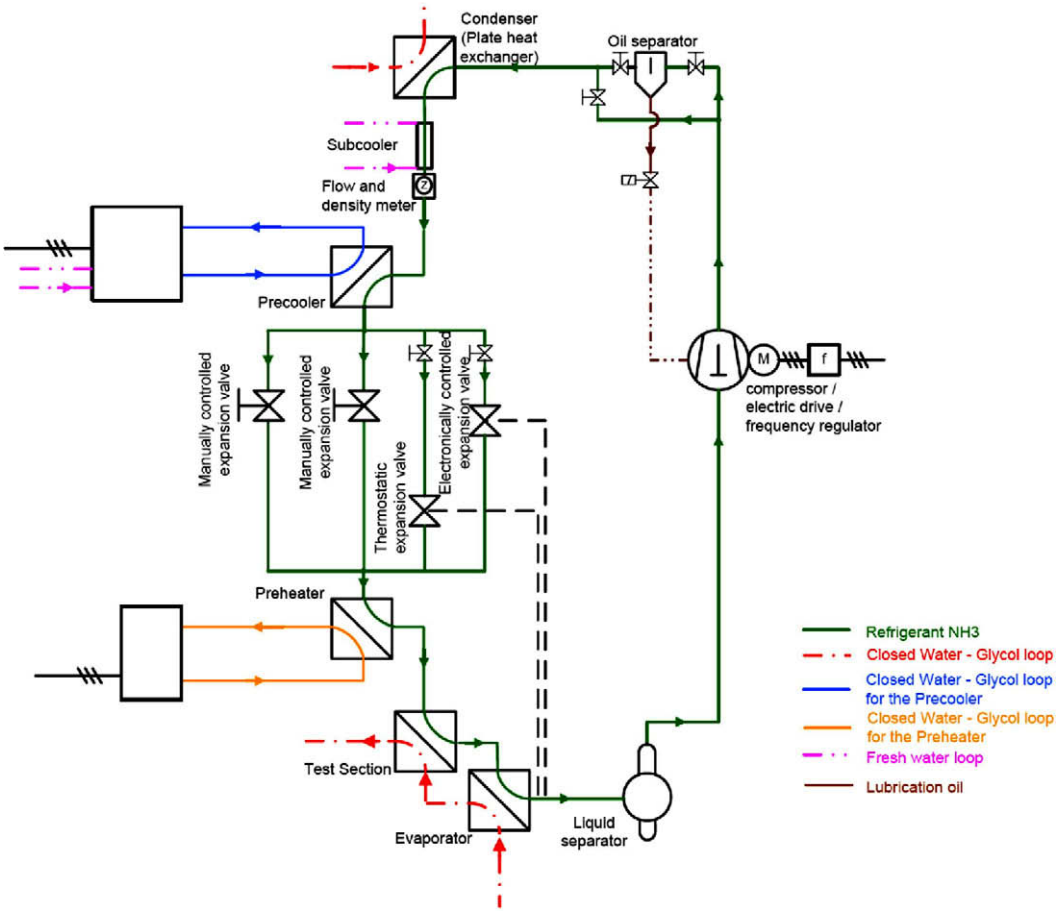


**Fig. 1.** Flow circuit schematics of the ammonia test facility.

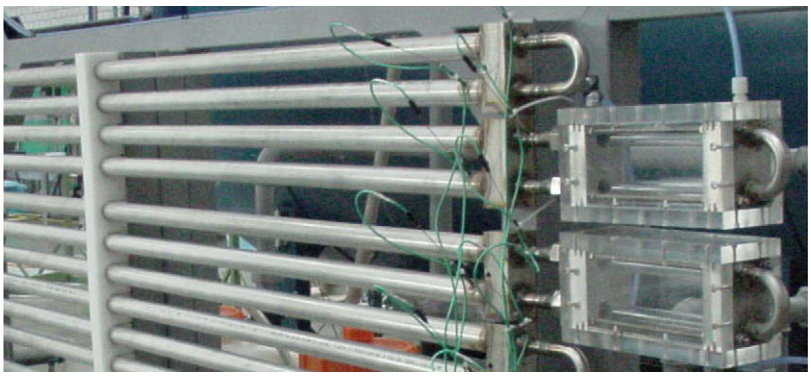

**Fig. 2.** Evaporator (before thermal insulation) with sight glasses.

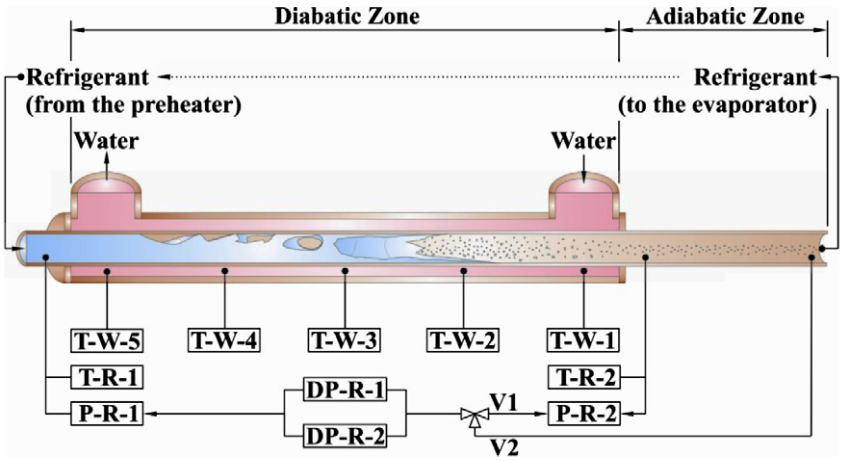


**Fig. 3.** Schematic of the horizontal test section.

**Table 2**
Measurement sections: number of thermocouples and axial position. The axial position is given in regards of the refrigerant flow.

| | Measurement sections | | | | | | |
|---|---|---|---|---|---|---|---|
| | T-R-1 | T-W-5 | T-W-4 | T-W-3 | T-W-2 | T-W-1 | T-R-2 |
| Number of thermocouples | 1 | 4 | 6 | 6 | 6 | 4 | 1 |
| Axial position (mm) | 0 | 34 | 534 | 1034 | 1534 | 1884 | 1918 |

The measurements, obtained with a National Instruments SCXI data acquisition system, are monitored and recorded with a Personal Computer. Each experimental point results from the average of 10 acquisition cycles. Each acquisition cycle corresponds to an average from 100 acquisitions made in approximately 0.02 s. All measurements were made at steady state conditions.

## 3. Measurements and data reduction

### 3.1. Saturation temperature

The saturation temperature $T$ of the fluid in the test section is obtained from the pressure measurements, using REFPROP [17], made at the extremities of each test section (diabatic and adiabatic), thus avoiding disturbing measurements with intrusive thermocouples. The end point measurements are corroborated by the inlet and outlet temperature measurements, *T-R*-1 and *T-R*-2, respectively, shown in Fig. 3.

### 3.2. Heat flux

The heat flux $q$ is controlled by the temperature of the hot water–glycol mixture. The temperature of the hot water–glycol mixture is measured at five positions along the test section (*T-W*-1, *T-W-2*, *T-W-3*, *T-W-4*, *T-W-5*), which allows its enthalpy profile to be determined:

$$h_{water}(z) = c_{p-water} T_{water}(z) \tag{1}$$

and thereby the heat flux profile:

$$q(z) = \frac{m_{water}}{\pi d} \frac{dh_{water}(z)}{dz} \tag{2}$$

The water–glycol mixture local temperature obtained at the measurement sections corresponds to the mean from four or six thermocouples circumferentially disposed in the annulus. The axial position $z$ of each measurement section and respective number of thermocouples is given in Table 2.

### 3.3. Vapor quality

The vapor quality $x$ is calculated by an energy balance over the preheater and the test section. Hence, the vapor quality at any position along the test section can be calculated from the following expression:

$$x(z) = \frac{Q_{preheater} + m_{water} c_{p-water}(T_{water(inlet)} - T_{water}(z))}{m_{ref} h_{LV-ref}(z)} \quad (3)$$

### 3.4. Pressure drop

The two-phase pressure drops are measured using two differential pressure transducers, *DP-R-1* and *DP-R-2*, each one covering different pressure drop ranges: low (0–10 mbar) and high (0–250 mbar). The pressure taps are placed at the top of the tube. The tubes connecting the pressure tap to the pressure transducer are submitted to the ambient temperature, and thus filled with vapor.

The total pressure drop of a fluid corresponds to the sum of three components: momentum, frictional and static head:

$$\Delta p_{total} = \Delta p_{momentum} + \Delta p_{frictional} + \Delta p_{static} \quad (4)$$

The flow is horizontal, thus $\Delta p_{static} = 0$, and therefore the frictional pressure drop is obtained by subtracting the momentum pressure drop from the measured pressure drop:

$$\Delta p_{frictional} = \Delta p_{total} - \Delta p_{momentum} \quad (5)$$

The momentum pressure drop reflects the increase in the kinetic energy of the flow during the evaporation process. For the diabatic flow, the momentum pressure drop is given by the following expression:

$$\Delta p_{momentum} = G^2 \left[ \frac{(1-x)^2}{\rho_L(1-\varepsilon)} + \frac{x^2}{\rho_G \varepsilon} \right]_{in}^{out} \quad (6)$$

where the void fraction $\varepsilon$ is calculated with the drift flux model of Rouhani [18]:

$$\varepsilon = \frac{x}{\rho_G} \left[ [1 + 0.12(1-x)] \left( \frac{x}{\rho_G} + \frac{1-x}{\rho_L} \right) + \frac{1.18(1-x)[g\sigma(\rho_L - \rho_G)]^{0.25}}{G\rho_L^{1/2}} \right] \quad (7)$$

Although the variation of the vapor quality $x$ along the diabatic test section is small, the evaluation of the momentum pressure drop is made by piecewise decomposition, between each water temperature measurement section.

The adiabatic frictional pressure drop corresponds to the pressure drop occurring in the adiabatic test section. This one is obtained from the difference between the total pressure drop in the test sections (valve in position *V2* in Fig. 3) and the diabatic pressure drop measured in the diabatic test section (valve in position *V1* in Fig. 3).

## 4. Uncertainties and reliability tests

### 4.1. Uncertainties

The measurement uncertainties were calculated taking into consideration the uncertainty of each element (summarized in Table 3) accordingly to a propagation of error analysis following the square root of the sum of the difference or *RSS* method [19]. The resulting maximum uncertainties do not exceed: 10% for the heat flux and 0.01 for the vapor quality. The pressure drop uncertainty is ±0.075% of the FS range of the differential pressure transducer for the diabatic data. For the adiabatic data, because it is obtained from the difference between the *V2* and *V1* measurements (see Fig. 3) the error is, following the *RSS* method, ±0.106% of the FS range of the differential pressure transducer.

**Table 3**
Parameter uncertainties.

| Parameter | Uncertainty |
|---|---|
| Temperature | ±0.03 °C |
| Mass flow | ±0.15% |
| Absolute pressure | ±20 mbar |
| Differential pressure (diabatic) | ±0.075% FS |

### 4.2. Validation tests

The validity of the test section, instrumentation and acquisition software was checked through single-phase liquid tests made before and after the experimental campaign. This allows the calibration of every single measuring element (mass flow rate, pressure and temperature) of the experimental set-up to be checked as well as the software running the acquisition and calculation functions. These tests concern a heat balance between water–glycol and subcooled refrigerant. These tests were performed for a range of saturation temperatures and mass velocities similar to those of the experimental campaign.

Fig. 4 depicts the energy balance ratio between heating water–glycol mixture and liquid ammonia, $Q_w/Q_r$, before and after the experimental campaign, for mass velocities ranging from 70 to 140 kg s$^{-1}$ m$^{-2}$ ($6080 < Re < 10{,}400$). As it is shown, the ratio of error ranges between a minimum value of −4% and a maximum value of 5%, with a mean error of only 2%, which is very accurate for these types of measurements. Also, there is no particular variation of the heat balance ratio between before and after the experimental campaign tests.

Furthermore, the absolute and differential pressure transducers were checked to verify that they gave a zero value for no flow. It was not possible however to measure the single-phase pressure drops as a validation as they were too small for the installed instrumentation whose measurement ranges were chosen for the larger two-phase values.

## 5. Flow pattern observations and comparison

### 5.1. Flow pattern map relationship to heat transfer and pressure drop models

As established by Kattan et al. [9], Baker [8] in 1954 was the first to recognize the importance of the flow pattern as a starting point

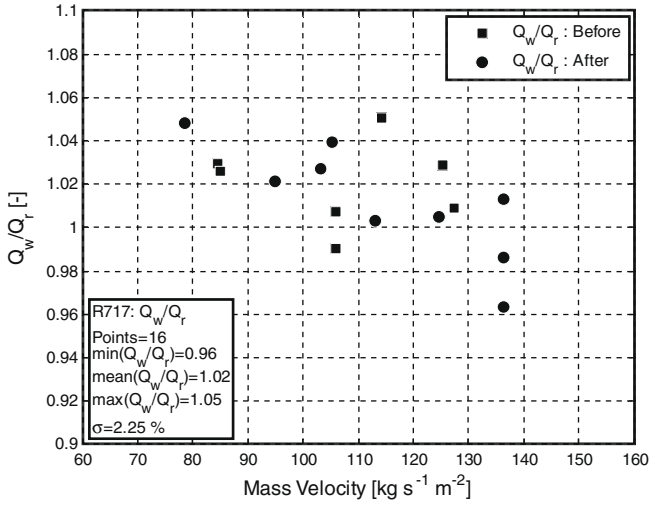


**Fig. 4.** Single-phase energy balance ratio, $Q_w/Q_r$, between heating water–glycol mixture and liquid ammonia.

for the calculation of heat and mass transfer, pressure drop and void fraction. Based in observations of flow patterns he developed an adiabatic flow pattern map for air–water. Also for air–water, Mandhane et al. [20] in 1975 developed an adiabatic flow pattern map that was compared to a large database. Later in 1976, Taitel and Dukler [21] proposed a new flow pattern based on their analytical analysis of the flow transition mechanisms together with empirical selection of several parameters. Hashizume [22] in 1983 proposed a revised version of the Baker map for refrigerants through the modification of the surface tension correction factor.

These flow pattern maps, although developed for horizontal adiabatic flows were often extrapolated for diabatic flows. A first step in including the influences of heat flux and dryout on the flow pattern transition boundaries was made by Kattan et al. [23] through the Kattan–Thome–Favrat flow pattern map, on which they based their heat transfer model [9,24]. The flow pattern map is based on experimental observations obtained for five refrigerants (single-component fluids: R134a and R123; zeotropic/near-azeotropes three-component mixture: R402A and R404A; and an azeotropic two-component mixtures: R502). This map consisted in a modified version of the Steiner [25] map, itself is a modified version of the Taitel–Dukler [21] map. Their map included a method for predicting the onset of dryout at the top of the tube in evaporating annular flows. Zürcher et al. [16] modified this map to better respect the ammonia observations, but these modifications required the entire set of equations to be iteratively solved to find the transition curves. Later, Thome and El Hajal [26] proposed an easier to implement version of the flow pattern map, avoiding iterative calculations. Finally, the most recent version of this flow pattern map model was proposed by Wojtan et al. [1]. This version, whose void fraction model was validated by dynamic void fraction measurements [27] made for R22 and R410A using a new interfacial measurement technique from Ursenbacher et al. [28], improved the accuracy of the former flow pattern map and added new *dryout* and *mist* flow boundaries. Based on their data and new flow pattern model, they proposed a new version of the flow pattern based heat transfer model [29].

Applying the same concept of flow pattern oriented models, El Hajal et al. [30] proposed a flow pattern map for condensation and Thome et al. [31] a flow pattern based model for condensation heat transfer. Furthermore Moreno Quibén and Thome [6] proposed a new flow pattern based frictional pressure drop model, while Cheng et al. [32,33] proposed a new flow pattern map, frictional pressure drop and heat transfer models for $CO_2$.

### 5.2. Observations

The flow pattern observations were made for three mass velocities/saturation temperatures combinations, for vapor qualities varying from 0.05 to 0.6. For the sake of simplicity, only the extremes cases are depicted and described here at the lower and higher mass velocities. The corresponding images were taken at the outlet of the preheater. All cases were compared to the flow pattern predictions of the flow pattern map of Wojtan et al. [1].

#### 5.2.1. $G = 50\ kg\ s^{-1}\ m^{-2}$, $T = -14\ °C$

Fig. 5 depicts images of several flow patterns observed during the experimental tests for the low mass velocity/saturation temperature case. The vapor quality increases from top to bottom in the images, depicting the effect of vapor quality on the flow structures. For this lower mass velocity case, the flow structures are mainly wavy-dominated. Because of that, for each condition two images are given, one captured with no wave (on the left) and the other (on the right) showing the passage of a large amplitude wave.

Fig. 5(a and b) shows the flow structure at a vapor quality of 0.11. It can be seen in Fig. 5(a) that the liquid layer is completely stratified at the bottom of the tube and its thickness varies as waves pass by. The height of the waves can be large as shown in Fig. 5(b), occasionally reaching the top of the tube. Whatever their height is, thin films are left behind on the wall tube, temporarily increasing the wetted angle $\theta_{wet}$. This flow structure is known as *slug-stratified wavy* flow in the flow pattern map of Wojtan et al. [1]. As the vapor quality increases to 0.21 in Fig. 5(c and d) the fluid velocity increases, making the bottom thickness decrease and the wetted angle increase. Comparison between Fig. 5(b) and (d) shows that the height of the waves decrease with increasing vapor quality. This flow structure is known as *slug-stratified wavy* flow. At a vapor quality of 0.30 in Fig. 5(e and f), the previous phenomena (wave height decrease and wetted perimeter increase) are amplified. As the waves no longer reach the top of the tube, the flow structure corresponds to *stratified-wavy* flow. Finally, Fig. 5(g and h) taken at a vapor quality of 0.41, show an additional amplification of the wetted perimeter and reduction of the bottom liquid layer thickness.

Further to the above comments, it can also be observed that the effect of the vapor quality increase is to increase the number of liquid droplets flowing along the top of the tube. Indeed, as the vapor quality increases, the velocity of the vapor phase increases, therefore increasing the number of droplets entrained on the top wall of the tube.

#### 5.2.2. $G = 100\ kg\ s^{-1}\ m^{-2}$, $T = -2\ °C$

For this case, observations were made at the outlet of the heater. At the lower vapor quality, $x = 0.05$, the thick liquid layer is completely stratified at the bottom of the tube with occasional large waves wetting the top of the tube. These large waves can be assimilated to form slugs of liquid and vapor. Indeed, as the mass velocity increases, slugs of vapor substitute these large waves of liquid. Thus, this flow pattern is called *slug-stratified-wavy*. At a vapor quality of 0.15 the entire perimeter of the tube is quasi-constantly wetted. The process is approaching the *annular* flow. At a vapor quality of 0.25 annular flow is establishing and from that vapor quality on, the flow pattern is *annular*.

#### 5.2.3. $G = 160\ kg\ s^{-1}\ m^{-2}$, $T = 12\ °C$

Fig. 6 is similar to Fig. 5, and depicts several flow pattern images that were observed for the high mass velocity/saturation temperature case. Again, the vapor quality increases from top to bottom images. Note that in this case only one image at each vapor quality is shown since the flow patterns are not modified by large amplitude waves.

Fig. 6(a) shows a characteristic slug of the *slug* flow pattern flow at a vapor quality of 0.07. The slugs intermittently wet the top perimeter of the tube. As the vapor quality increases, the slug frequency increases, leading to the transition to *intermittent* flow, as shown in Fig. 6(b) at a vapor quality of 0.21. Increasing the vapor quality further to 0.29, an internal vapor core starts taking form, leading the flow structure into the transition from *intermittent* to *annular* flow, as shown in Fig. 6(c). Finally, as the vapor quality is increased to 0.41, *annular* flow is established as shown in Fig. 6(d). Note that interfacial waves on the annular film are clearly visible.

### 5.3. Comparison to the model of Wojtan et al. [1]

Fig. 7 depicts the predicted flow transitions of the Wojtan et al. [1] flow pattern map for the same experimental conditions as for the flow pattern observations. The horizontal lines indicate the

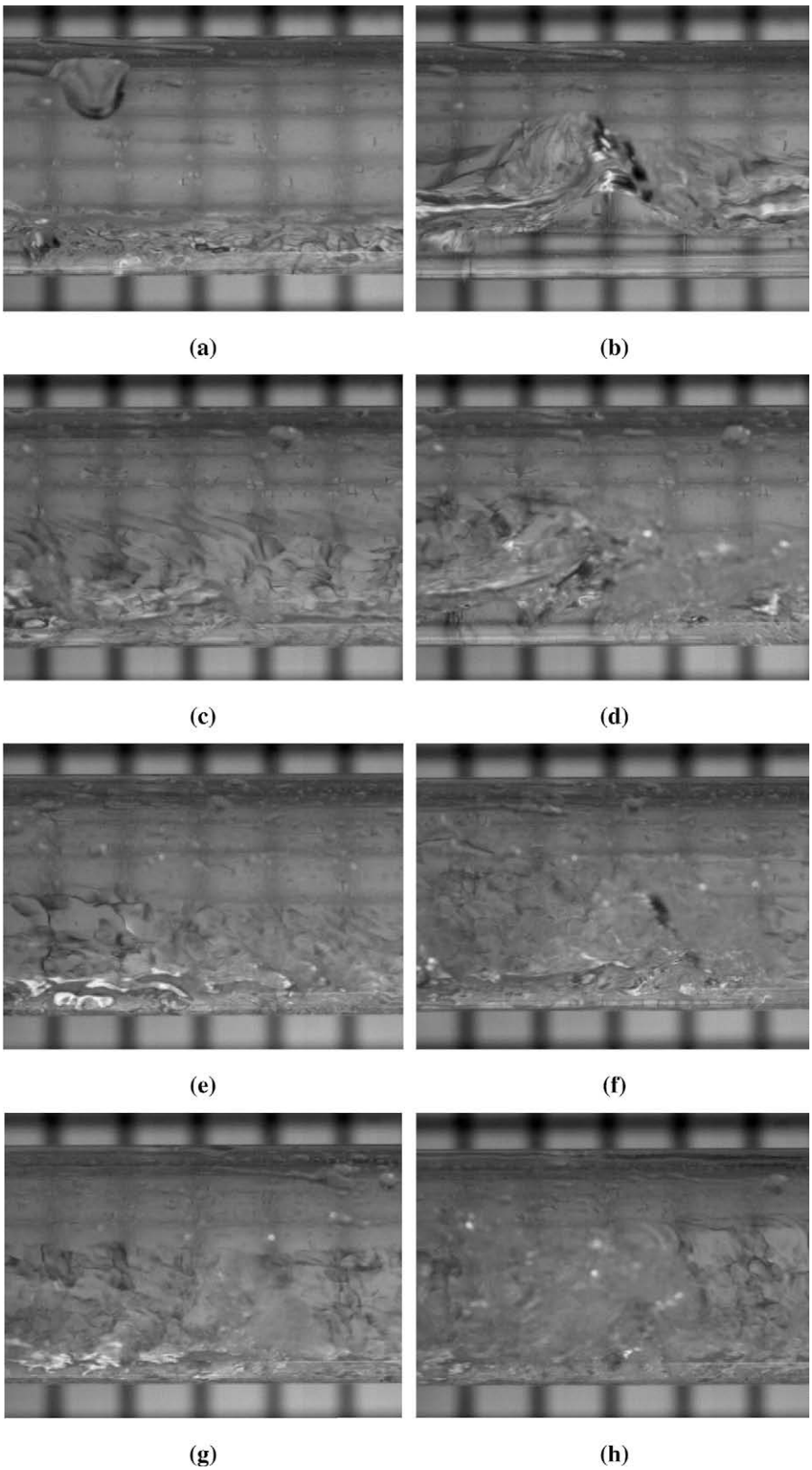


**Fig. 5.** Flow pattern observations with ammonia flowing inside a 14-mm ID smooth glass tube at several vapor qualities for $G = 50$ kg s$^{-1}$ m$^{-2}$ and $T = -14$ °C. Vapor quality $x$ increases from top to bottom: (a and b) $x = 0.11$, (c and d) $x = 0.21$, (e and f) $x = 0.30$, (g and h) $x = 0.41$. Images on left were captured with no wave, while those on the right were captured when a large wave was passing.

flow process path corresponding to the respective mass velocity, while the other lines indicate the flow pattern boundaries of the flow pattern map. The markers indicate the vapor quality at which the observations were made and its respective observed flow

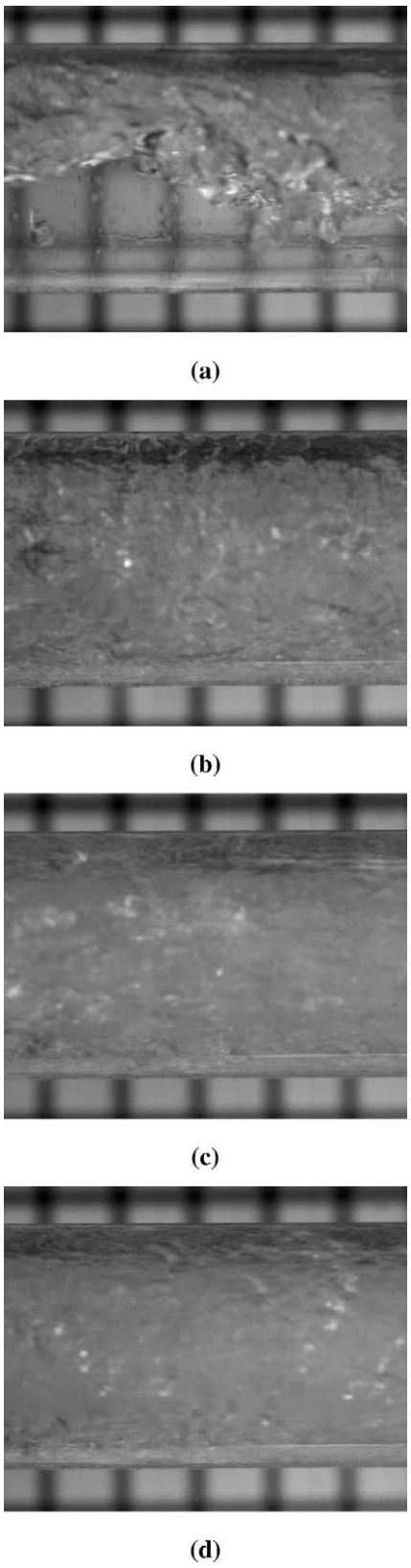


**Fig. 6.** Flow pattern observations with ammonia flowing inside a 14-mm ID smooth glass tube at several vapor qualities with $G = 160\ \mathrm{kg\,s^{-1}\,m^{-2}}$ and $T = 12\ ^{\circ}\mathrm{C}$. Vapor quality increases from top to bottom: (a) $x = 0.07$, (b) $x = 0.21$, (c) $x = 0.29$, (d) $x = 0.41$.

pattern. The comparison between the observations and map gives very good results, as the map correctly predicts almost 100% of the flow pattern observations.

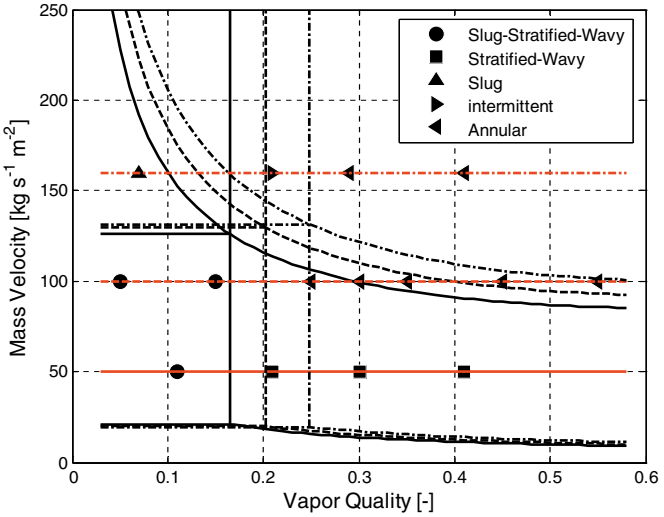


**Fig. 7.** Flow pattern map of Wojtan **et al**. [1] for ammonia flowing inside a 14-mm ID smooth tube for the observation experimental conditions. Solid lines correspond to $G = 50\ \mathrm{kg\,s^{-1}\,m^{-2}}$ and $T = -14\ ^{\circ}\mathrm{C}$ dashed lines correspond to $G = 100\ \mathrm{kg\,s^{-1}\,m^{-2}}$ and $T = -2\ ^{\circ}\mathrm{C}$, and dotted lines correspond to $G = 160\ \mathrm{kg\,s^{-1}\,m^{-2}}$ and $T = 12\ ^{\circ}\mathrm{C}$.

For the low mass velocity, all the flow patterns observed correspond to the predictions of the model. For the intermediate flow mass velocity, only three observations are not accurately predicted: *annular* flow was observed instead of *stratified-wavy*, at vapor qualities of 0.25, 0.30 and 0.35. Indeed, for this intermediate mass velocity, these vapor qualities stand close between two flow pattern transition boundaries, namely *intermittent*-to-*stratified-wavy* and *stratified-wavy*-to-*annular*, which are not line-wise but band-wise. For the high mass velocity case, all flow patterns observed correspond to the predictions of the map.

## 6. Experimental frictional pressure drop results

The frictional pressure drop results are divided into two groups in function of their process path (mass velocity): passing (or not) through the annular flow pattern (higher or lower than the minimum mass velocity of the *annular*-to-*stratified-wavy* flow transition boundary), according to the flow pattern map of Wojtan et al. [1]. Fig. 8 depicts the flow pattern map for three test conditions of combined mass velocity and saturation temperature: low, medium and high. The solid circles indicate the minimum mass velocity of the *annular*-to-*stratified-wavy* flow transition boundary. For example, for $G = 55\ \mathrm{kg\,s^{-1}\,m^{-2}}$, Fig. 8 shows that the process path will never cross *annular* flow as this mass velocity is lower than the corresponding minimum of the *annular*-to-*stratified wavy* flow transition boundary (indicated by a circle). On the other hand, for $G = 160\ \mathrm{kg\,s^{-1}\,m^{-2}}$, Fig. 8 shows that the process path will cross *annular* flow as the mass velocity is higher than the corresponding minimum mass velocity. It is important to note that the predictions of the flow pattern model of Wojtan et al. [1] showed very good agreement with the flow pattern observations.

Fig. 9 depicts the frictional pressure gradients of ammonia flowing inside the 14 mm ID smooth and horizontal stainless steel tube for mass velocities (a) lower and (b) higher than the minimum mass velocity of the *annular*-to-*stratified-wavy* boundary of the flow pattern map model of Wojtan et al. [1]. For both conditions of mass velocity, it can be seen that the frictional pressure gradient increases with the vapor quality. As the vapor quality increases, the flow is accelerated to a higher velocity and thus the pressure drop increases. Naturally, as the mass velocity increases, the pressure gradient increases too.

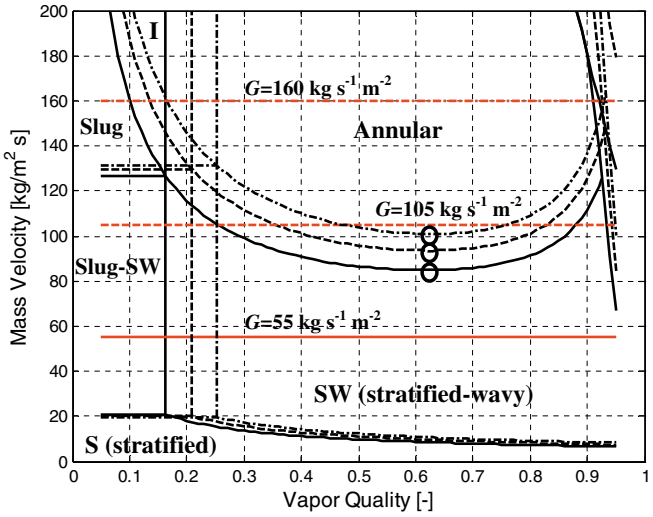


**Fig. 8.** Flow pattern map for ammonia flow boiling in a smooth tube, 14 mm ID for three combined sets of mass velocity and saturation temperature: low (solid lines, $G = 55$ kg/s m$^2$, $T = -14$ °C, $q = 12$ kW m$^{-2}$), medium (dashed lines, $G = 105$ kg/s m$^2$, $T = 0$ °C, $q = 12$ kW m$^{-2}$), and high (dot–dashed lines, $G = 160$ kg/s m$^2$, $T = 13$ °C, $q = 12$ kW m$^{-2}$). Red horizontal lines represent the process path. Solid circles represent the minimum mass velocity of the *annular*-to-*stratified wavy* flow transition boundary. Letters represent their respective flow pattern: I, intermittent; S, stratified; SW, stratified-wavy.

It is important to note that the effect of the saturation temperature on the frictional pressure drop is opposite to that of the mass velocity: increasing the saturation temperature decreases the frictional pressure drop. This is due to the physical properties of the fluid, as the saturation temperature increases, the liquid to vapor density and viscosity ratios decrease and thereby, the frictional pressure drop decreases. However, the experimental results show that the frictional pressure gradient increases with the increase of mass velocity and saturation temperature. Therefore, it can be concluded that, for the variations of the combined set of mass velocity and saturation temperature presented here, the effect of the mass velocity overcomes that of the saturation temperature.

Neglecting the effect of the saturation temperature, it can be seen that for the low mass velocity case, a 72% of variation of mass velocity (from 55 to 90 kg s$^{-1}$ m$^{-2}$) causes about a 100% increase in the pressure drop. For the higher mass velocity case, a 52% of variation of mass velocity (from 105 to 160 kg s$^{-1}$ m$^{-2}$) causes about a 45% increase in the pressure drop.

Fig. 10 shows the experimental frictional pressure gradient results for both diabatic and adiabatic conditions. For the sake of simplicity, only the higher, medium and lower mass velocity cases are shown, but the trends in this figure were observed for all the experimental conditions of this study. It can be seen that there is a very good agreement between the adiabatic and diabatic frictional pressure gradients, showing that the evaporation process itself does not influence the frictional pressure gradient. This also attests to the accuracy and reliability of the measurements as well as the data reduction procedure.

## 7. Assessment of prediction methods

The existing frictional pressure drop prediction methods can be divided into three main categories: empirical, analytical and phenomenological. In what follows, the first and last of these types are commented on and compared with the experimental data. The equations of the methods are summarized in Table 5. Analytical/numerical methods are beyond the scope of the present study.

### 7.1. Empirical methods

Empirical methods, generally very simple to apply, are based on a minimum knowledge of the flow characteristics and are strongly dependent on the composition of the databanks used for their development. Due to their simplicity, they are not general, and thus, their application is restricted to a limited range of conditions. However, they usually offer good prediction accuracy within those boundaries.

Methods such as those from Lockhart and Martinelli [3], Bankoff [34], Cicchitti et al. [35], Thom [36], Pierre [37], Baroczy [38], Chawla [39], Chisholm [40], Friedel [2], Grönnerud [5], Müller-Steinhagen and Heck [4] are examples of empirical methods.

Ould-Didi et al. [41] compared leading methods to experimental pressure drops obtained for five different refrigerants (R134a, R123, R402a, R404A and R502) over a wide range of experimental conditions. Overall, they found the methods of Grönnerud [5] and Müller-Steinhagen and Heck [4] to give the best performance, while the correlation of Friedel [2] was the third best in a comparison to five

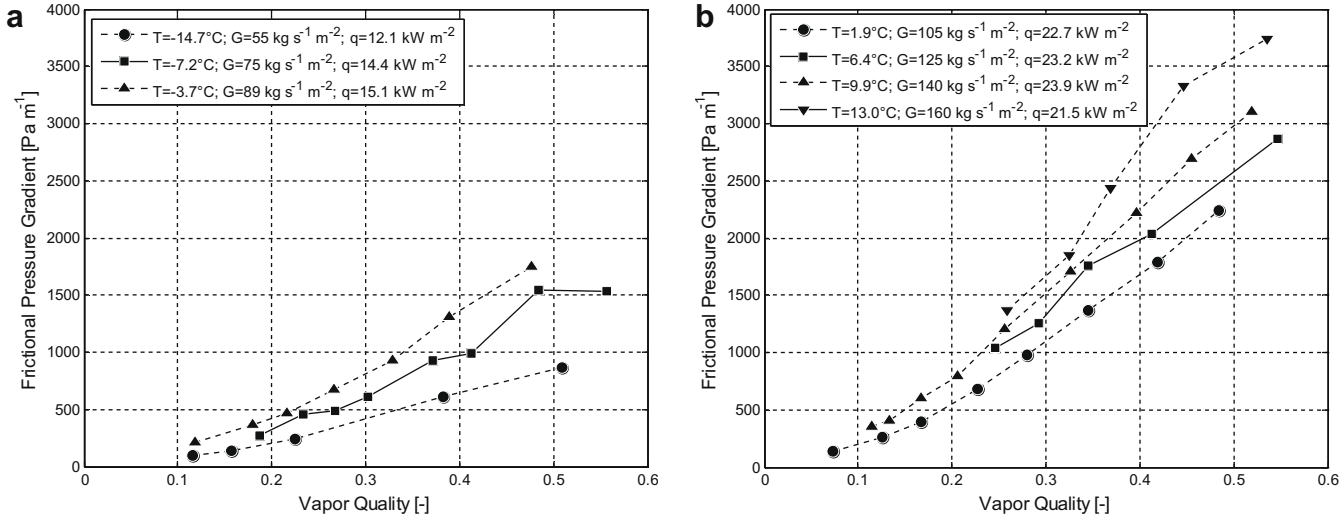


**Fig. 9.** Frictional pressure gradients of ammonia for high heat flux and mass velocities (a) lower and (b) higher than the minimum mass velocity of the *annular*-to-*stratified-wavy* boundary of the flow pattern map model of Wojtan **et al.** [1].

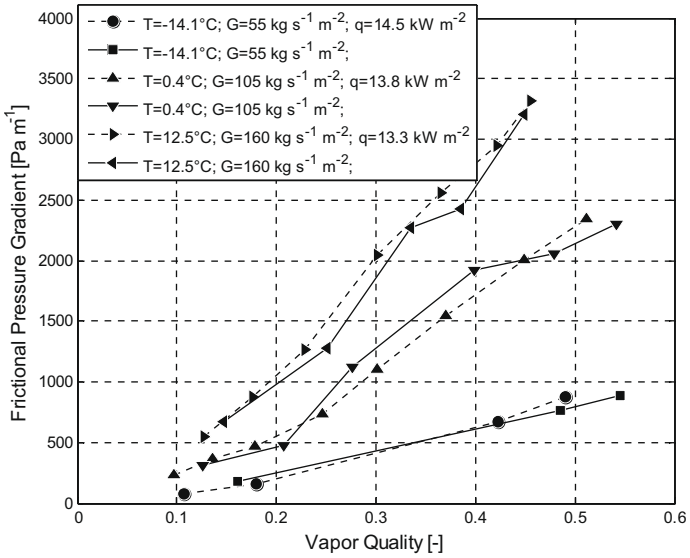


**Fig. 10.** Adiabatic and diabatic frictional pressure gradients of ammonia for high, medium and low mass velocities.

leading methods (Lockhart and Martinelli [3], Friedel [2], Grönnerud [5], Chisholm [40], Müller-Steinhagen and Heck [4]).

Moreno Quibén and Thome [6] compared their database (Moreno Quibén and Thome [42]) covering three fluids (R134a, R22 and R410A) against the correlations of Müller-Steinhagen and Heck [4], Grönnerud [5] and Friedel [2]. They concluded that, from the three correlations, Müller-Steinhagen and Heck [4] was the one predicting the best with 76% of the predicted values within ±30%. Still, the new phenomenological model of Moreno Quibén and Thome [6] predicted almost 10% better than the correlation of Müller-Steinhagen and Heck [4] within the ±30% error band and 15% better within ±20% error.

While these comparisons show that the correlations of Grönnerud [5] and Müller-Steinhagen and Heck [4] are generally predicting refrigerants reasonably well, they do not give any information on the prediction accuracy relative to ammonia data.

Thome et al. [11] compared experimental data from Shah [12] and Kabelac and De Buhr [15] to the correlations of Chisholm [40], Friedel [2] and Müller-Steinhagen and Heck [4] and Moreno Quibén and Thome [6]. It was observed that no method could accurately predict all these databases. The best overall prediction was 51% inside an error window of ±30% by the phenomenological model of Moreno Quibén and Thome [6].

In this study, the empirical methods of Chawla [39], Chisholm [40], Cicchitti et al. [35], Bankoff [34], Grönnerud [5], Friedel [2] and Müller-Steinhagen and Heck [4] were compared to the experimental data. Comparison to those of Chawla [49], Cicchitti et al. [35] and Bankoff [34] resulted in a very low level of accuracy (less than 50% within ±30%), and thus, details of these results are omitted.

Fig. 11 shows the comparison of the experimental data to the predicted results of the methods of (a) Friedel [2] and (b) Müller-Steinhagen and Heck [4]. It can be seen that both Friedel [2] and Müller-Steinhagen and Heck [4] produce the same type of trend. In the low vapor quality region, the frictional pressure gradient is over-predicted. As the values of the pressure gradient increase, these methods tend to decrease the over-estimation and finally end with major under-estimations of over 40%. Despite that, the methods of Friedel [2] and Müller-Steinhagen and Heck [4] predict 55 and 60%, respectively, of the experimental data inside a ±30% error window. The correlation of Müller-Steinhagen and Heck [4] predicts the data with less deviation than that of Friedel [2], 39% and 56%, respectively, but their absolute mean error ranges between 41% and 30%, respectively. While the correlation of Müller-Steinhagen and Heck [4] is based on a two-phase interpolation of liquid and vapor frictional pressure drops, the correlation of Friedel [2] is a function of the liquid frictional pressure drop and empirical factors that takes into account the vapor properties, vapor quality, etc.

The methods of Lockhart and Martinelli [3] and of Grönnerud [5] reproduce the data with a different trend than that observed with the two previous correlations. The correlation of Lockhart and Martinelli [3] still tends to over-predict the experimental data in the low vapor quality domain. Although presenting a higher level of dissipation, statistically, it keeps a standard deviation of 53%, which is of the same order as that of Friedel [2]. This correlation predicts the experimental data with a limited accuracy, i.e., 52% of the data within ±30% error. Fig. 12 shows the comparison.

The correlation of Grönnerud [5], although under-estimating the experimental data (mean error of −16%), presents the best accuracy for this category of methods. It predicts 93% of the experimental data inside the ±30% error boundaries while maintaining a low level of dissipation, as its standard deviation is only 11%, which is also the best of this category. Note that the number of experimental data predicted inside an error window of ±20% is higher than that predicted inside an error window of ±30% obtained with the other empirical correlations.

### 7.2. Phenomenological methods

Phenomenological methods, more complicated to apply than empirical methods, are based on a theoretical approach of the flow characteristics. However, they still require experimental data to fix empirical constants, as well as an accurate flow pattern map to predict when to use the different interfacial structures. They generally are expected to provide a better prediction accuracy than wholly empirical methods.

Many phenomenological methods exist, but they are generally restricted to a particular flow pattern or range of flow conditions, for example: the methods of Cheremisinoff and Davis [43], Chen and Spedding [44] and Kadambi [45] have been applied to *stratified* flow; the methods of Dukler and Hubbard [46] and Kordbyan [47] have been applied to *slug* flow and the methods of Hoogendoorn [48], Wallis [49] and Hashizume [50] have been applied to *annular* flow. Other methods can only be applied within a specific range of conditions, such as that of Hart et al. [51], the apparent rough surface or ARS model, which can only be applied within a range

**Table 4**
Summary of the statistical analysis of the comparisons, segregated by flow pattern for diabatic, adiabatic and overall conditions. Lowercase a, d and t stand for adiabatic, diabatic and total, respectively. Shaded cells indicated the best results for each statistical element.

| Low patterns | Nbr. of points | | | Statistical elements | | | Models | | | | | | | | | | | | | |
|---|---|---|---|---|---|---|---|---|---|---|---|---|---|---|---|---|---|---|---|---|
| | | | | | | | Empirical | | | | | | | | | | | | Phenomenological Moreno Quibén and Thome [6] | | |
| | | | | | | | Lockhart and Martinelli [3] | | | Friedel [2] | | | Grönnerud [5] | | | Müller-Steinhagen and Heck [4] | | | | | |
| | a | d | t | | | | a | d | t | a | d | t | a | d | t | a | d | t | a | d | t |
| Stratified- wavy | 37 | 40 | 77 | Mean error | | | 19.8 | 19.9 | 19.9 | 18.9 | 16.5 | 17.7 | −16.1 | −18.9 | −17.6 | 9.6 | 6.7 | 8.1 | 9.8 | 5.3 | 7.5 |
| | | | | Abs mean error | | | 34.5 | 33.5 | 34.0 | 29.9 | 28.2 | 29.0 | 17.0 | 19.1 | 18.1 | 23.1 | 21.6 | 22.3 | 14.2 | 7.3 | 10.6 |
| | | | | Standard deviation | | | 39.1 | 38.5 | 38.8 | 37.8 | 38.2 | 38.0 | 10.1 | 7.9 | 9.1 | 29.5 | 29.4 | 29.5 | 13.3 | 7.9 | 11.1 |
| | | | | Points inside an | ±20 | % | 32.4 | 40.0 | 36.4 | 51.4 | 52.5 | 51.9 | 70.3 | 42.5 | 55.8 | 56.8 | 60.0 | 58.4 | 75.7 | 97.5 | 87.0 |
| | | | | error window of | ±30 | | 45.9 | 50.0 | 48.1 | 70.3 | 72.5 | 71.4 | 83.8 | 97.5 | 90.9 | 78.4 | 82.5 | 80.5 | 94.6 | 100.0 | 97.4 |
| Slug- stratified- wavy | 14 | 29 | 43 | Mean error | ±20 | | 85.5 | 114.2 | 104.9 | 67.9 | 105.7 | 93.4 | −8.4 | −5.1 | −6.2 | 39.0 | 59.9 | 53.1 | 1.9 | 2.6 | 2.4 |
| | | | | Abs mean error | | | 86.8 | 114.2 | 105.3 | 71.9 | 105.7 | 94.7 | 15.0 | 8.8 | 10.8 | 44.3 | 60.1 | 54.9 | 16.5 | 9.6 | 11.9 |
| | | | | Standard deviation | | | 37.5 | 39.3 | 41.0 | 38.6 | 61.9 | 58.2 | 18.0 | 8.9 | 12.7 | 30.7 | 40.6 | 38.9 | 20.1 | 11.3 | 14.7 |
| | | | | Points inside an | ±20 | % | 7.1 | 0.0 | 2.3 | 0.0 | 3.4 | 2.3 | 85.7 | 96.6 | 93.0 | 21.4 | 17.2 | 18.6 | 64.3 | 89.7 | 81.4 |
| | | | | error window of | ±30 | | 7.1 | 0.0 | 2.3 | 14.3 | 3.4 | 7.0 | 85.7 | 100.0 | 95.3 | 21.4 | 24.1 | 23.3 | 85.7 | 100.0 | 95.3 |
| Slug | 3 | 7 | 10 | Mean error | | | 47.3 | 108.0 | 89.8 | 15.2 | 67.5 | 51.8 | −26.5 | −5.3 | −11.6 | −6.0 | 29.9 | 19.1 | −21.6 | −2.5 | −8.2 |
| | | | | Abs mean error | | | 47.3 | 108.0 | 89.8 | 19.9 | 67.5 | 53.2 | 26.5 | 6.5 | 12.5 | 15.4 | 29.9 | 25.5 | 21.6 | 6.6 | 11.1 |
| | | | | Standard deviation | | | 27.2 | 25.4 | 38.1 | 20.0 | 23.5 | 32.9 | 12.5 | 6.2 | 13.0 | 15.1 | 14.2 | 21.9 | 10.0 | 7.5 | 12.1 |
| | | | | Points inside an | ±20 | % | 33.3 | 0.0 | 10.0 | 66.7 | 0.0 | 20.0 | 33.3 | 100.0 | 80.0 | 66.7 | 28.6 | 40.0 | 33.3 | 100.0 | 100.0 |
| | | | | error window of | ±30 | | 33.3 | 0.0 | 10.0 | 66.7 | 14.3 | 30.0 | 33.3 | 100.0 | 80.0 | 100.0 | 42.9 | 60.0 | 66.7 | | 90.0 |
| Intermittent | 2 | 5 | 7 | Mean error | | | 27.7 | 55.6 | 47.6 | −1.6 | 15.5 | 10.6 | −26.8 | −12.1 | −16.3 | −14.5 | −1.1 | −4.9 | −14.8 | −2.5 | −6.0 |
| | | | | Abs mean error | | | 27.7 | 55.6 | 47.6 | 20.4 | 17.0 | 18.0 | 26.8 | 12.1 | 16.3 | 17.5 | 7.6 | 10.4 | 15.5 | 5.6 | 8.4 |
| | | | | Standard deviation | | | 25.5 | 15.0 | 22.5 | 20.4 | 12.2 | 16.9 | 13.9 | 4.9 | 10.8 | 17.5 | 8.9 | 13.4 | 15.5 | 6.1 | 11.2 |
| | | | | Points inside an | ±20 | % | 50.0 | 0.0 | 14.3 | 50.0 | 60.0 | 57.1 | 50.0 | 100.0 | 85.7 | 50.0 | 100.0 | 85.7 | 50.0 | 100.0 | 85.7 |
| | | | | error window of | ±30 | | 50.0 | 0.0 | 14.3 | 100.0 | 100.0 | 100.0 | 50.0 | 100.0 | 85.7 | 50.0 | 100.0 | 85.7 | 50.0 | 100.0 | 85.7 |
| Annular | 42 | 43 | 85 | Mean error | | | −2.8 | −4.9 | −3.9 | −22.6 | −24.7 | 23.7 | −17.3 | −20.0 | −18.6 | −25.8 | −27.8 | −26.8 | 5.2 | 2.2 | 3.7 |
| | | | | Abs mean error | | | 17.5 | 14.4 | 15.9 | 24.0 | 24.9 | 24.5 | 17.3 | 20.0 | 18.6 | 26.0 | 27.8 | 26.9 | 10.5 | 4.1 | 7.3 |
| | | | | Standard deviation | | | 20.8 | 15.7 | 18.4 | 14.6 | 10.7 | 12.8 | 8.8 | 4.7 | 7.2 | 11.8 | 7.8 | 10.1 | 11.1 | 5.0 | 8.7 |
| | | | | Points inside an | ±20 | % | 64.3 | 74.4 | 69.4 | 35.7 | 25.6 | 30.6 | 61.9 | 41.9 | 51.8 | 28.6 | 18.6 | 23.5 | 90.5 | 100.0 | 95.3 |
| | | | | error window of | ±30 | | 83.3 | 95.3 | 89.4 | 66.7 | 58.1 | 62.4 | 92.9 | 100.0 | 96.5 | 64.3 | 51.2 | 57.6 | 100.0 | 100.0 | 100.0 |
| Overall | 98 | 124 | 222 | Mean error | | | 20.5 | 39.8 | 31.3 | 7.6 | 25.9 | 17.8 | 16.0 | 15.0 | 15.5 | 2.3 | 8.2 | 3.5 | 5.2 | 2.9 | 3.9 |
| | | | | Abs mean error | | | 34.9 | 50.8 | 43.8 | 32.9 | 47.0 | 40.7 | 17.3 | 16.0 | 16.6 | 27.0 | 32.7 | 30.2 | 13.2 | 6.6 | 9.5 |
| | | | | Standard deviation | | | 43.1 | 58.0 | 52.8 | 42.8 | 62.9 | 55.7 | 11.9 | 9.6 | 10.7 | 32.7 | 42.5 | 38.8 | 15.0 | 8.2 | 11.8 |
| | | | | Points inside an | ±20 | % | 42.9 | 38.7 | 40.5 | 37.8 | 29.0 | 32.9 | 67.3 | 60.5 | 63.5 | 39.8 | 35.5 | 37.4 | 78.6 | 96.8 | 88.7 |
| | | | | error window of | ±30 | | 56.1 | 49.2 | 52.3 | 61.2 | 49.2 | 54.5 | 85.7 | 99.2 | 93.2 | 64.3 | 56.5 | 59.9 | 93.6 | 100 | 97.3 |

Error: $\varepsilon_i = (h_{pred,i} - h_{exp,i})/h_{exp,i}$ (8)

Mean error: $\bar{\varepsilon} = \frac{1}{n}\sum_{i=1}^{n}\varepsilon_i$ (9)

Absolute mean error: $|\bar{\varepsilon}| = \frac{1}{n}\sum_{i=1}^{n}|\varepsilon_i|$ (10)

Standard deviation $\sigma = \sqrt{\frac{1}{n}\sum_{i=1}^{n}(\varepsilon_i - \bar{\varepsilon})^2}$ (11)

**Table 5**
Summary of the models compared against the experimental data. For the sake of simplicity, the frictional pressure drop model of Moreno Quibén and Thome [6] and flow pattern model of Wojtan **et al**. [1] are not included.

| Category | Correlation | | | | | | | |
|---|---|---|---|---|---|---|---|---|
| Empirical | Friedel [2] | $\Delta p_f = \Delta p_{LO}\phi_{LO}^2$ | (12) | $F = x^{0.78}(1-x)^{0.224}$ | (14) | $H = (\frac{\rho_L}{\rho_G})^{0.91}(\frac{\mu_G}{\mu_L})^{0.19}(1-\frac{\mu_G}{\mu_L})^{0.7}$ | | (16) |
| | | $\phi_{LO}^2 = E + \frac{3.24FH}{Fr_H^{0.045}We_L^{0.035}}$ | (13) | $E = (1-x)^2 + x^2\frac{\rho_L f_G}{\rho_G f_L}$ | (15) | | | |
| | Lockhart and Martinelli [3] | $\Delta p_f = \Delta p_L \phi_{Ltt}^2$ | (17) | $X_{tt} = (\frac{1-x}{x})^{0.9} + (\frac{\rho_G}{\rho_L})^{0.5} + (\frac{\mu_L}{\mu_G})^{0.1}$ | (21) | | | |
| | | $\phi_{Ltt}^2 = 1 + \frac{C}{X_{tt}} + \frac{1}{X_{tt}^2}$ Re$_L$ > 4000 | (18) | | | | | |
| | | $\Delta p_f = \Delta p_G \phi_{Gtt}^2$ | (19) | | | | | |
| | | $\phi_{Gtt}^2 = 1 + CX_{tt} + X_{tt}^2$ Re$_L$ < 4000 | (20) | | | | | |
| | Müller-Steinhagen and Heck [4] | $(\frac{dp}{dz})_f = K(1-x)^{1/3} + (\frac{dp}{dz})_{G0}x^3$ | (22) | $K = (\frac{dp}{dz})_{L0} + 2((\frac{dp}{dz})_{G0} - (\frac{dp}{dz})_{L0})x$ | (23) | | | |
| | Grönnerud [5] | $\Delta p_f = \Delta p_{LO}\phi_{Gd}$ | (24) | $\phi_{Gd} = 1 + (\frac{dp}{dz})_{Fr}[\frac{(\frac{\rho_L}{\rho_G})}{(\quad)}\frac{\mu_L}{\mu_G}^{0.25} - 1]$ | (25) | $(\frac{dp}{dz})_{Fr} = f_{Fr}[x + 4(x^{1.8} - x^{10}f_{Fr}^{0.5})]$ | | (26) |
| | | | | | | $Fr_L < 1 f_{Fr} = Fr_L^{0.3} + 0.0055[\ln(\frac{1}{Fr_L})]^2 Fr_L \geq 1 f_{Fr} = 1$ | | (27) |

| Liquid | Vapor | C |
|---|---|---|
| Laminar | Laminar | 5 |
| Laminar | Turbulent | 12 |
| Turbulent | Laminar | 10 |
| Turbulent | Turbulent | 20 |

| | | | | | | | | | | |
|---|---|---|---|---|---|---|---|---|---|---|
| Phenomenological | Moreno Quibénand Thome [6] | | The implementation of this model requires the flow pattern map model of Wojtan et al. [1]. For the sake of simplicity the description of both methods, flow pattern map model and frictional pressure drop model, is avoided here. It is recommended to consult the respective articles. | | | | | | | |
| The pressure gradient for a single-phase flow is given by: | $(\frac{dp}{dz})_{i0} = f_i\frac{2G^2}{d\rho_i}$ | (28) | The liquid and vapor pressure drop in a two-phase flow is given by: | $\Delta p_L = 4f_L\frac{L}{d}G^2\frac{(1-x)^2}{2\rho_L}$ | (29) | And the friction factor is calculated in function of the Reynolds number: | Re < 2000 : $f_i = \frac{16}{\text{Re}_i}$ | (31) | Where the Reynolds number of each phase *i* is: | Re$_i = \frac{Gd}{\mu_i}$ (33) |
| | | | | $\Delta p_G = 4f_G\frac{L}{d}G^2\frac{x^2}{2\rho_G}$ | (30) | | Re > 2000 : $f = \frac{0079}{\text{Re}^{0.25}}$ | (32) | | |
| The liquid Webber number is calculated with: | $We_L = \frac{G^2 d}{\sigma\rho_H}$ | (34) | The homogeneous density is calculated with: | $\rho_H = (\frac{x}{\rho_G} + \frac{1-x}{\rho_L})^{-1}$ | (35) | The Froud number is calculated with: | $Fr_i = \frac{G^2}{gd\rho_i}^2$ | (36) | | |

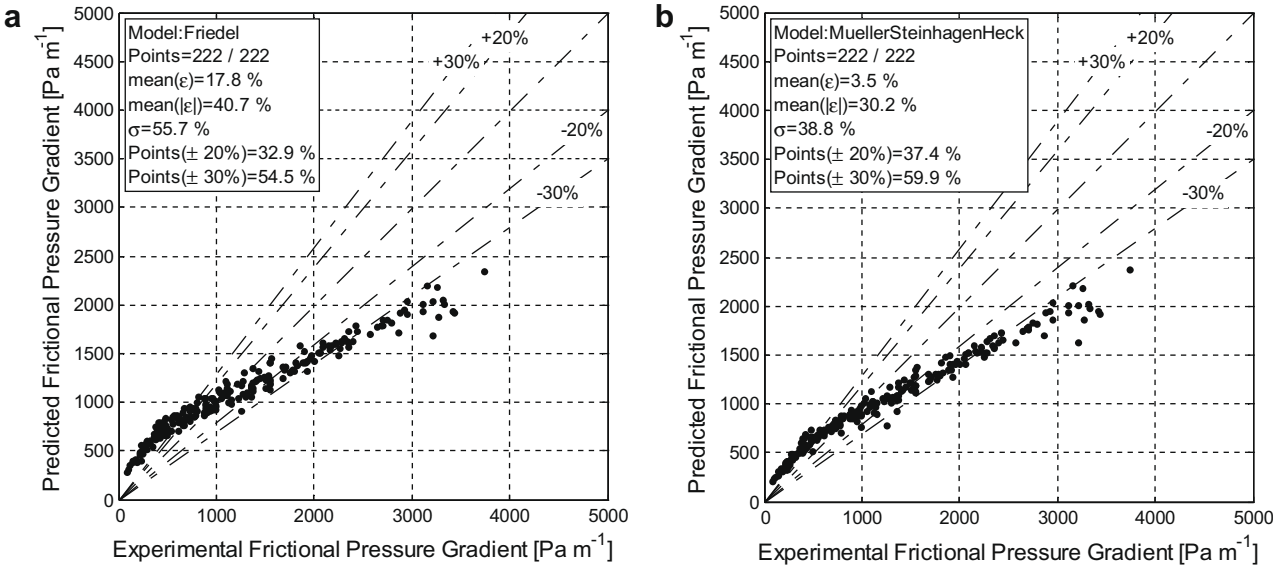


**Fig. 11.** Comparison of the experimental data to the predicted results of the models of (a) Friedel [2] and (b) Müller-Steinhagen and Heck [4].

of high values of void fraction ($0.94 < \varepsilon < 1$). This observation preludes one of the major difficulties in following this approach, that is, they need a very reliable flow pattern map in order to be able to predict the different interfacial structures and the transitions from one regime to another.

Moreno Quibén and Thome [6] presented a new frictional pressure gradient model that covers all the flow patterns in the flow pattern map of Wojtan et al. [1]. Developed and based on results for halocarbons R22, R134a and R410A from [42], this model was recently modified to work also at very high pressures for $CO_2$ by Cheng et al. [32] and it is compared to the present experimental data for ammonia.

The results indicate that the predictions are well centered as the mean error is only 3.9%. Most of the data are contained inside the ±20% window and 97% of the experimental data are within the ±30% error range. Fig. 13 shows the comparison. Although with a slightly higher value of standard deviation than that of Grönnerud, the model of Moreno Quibén and Thome gives the best prediction accuracy of all the tested methods.

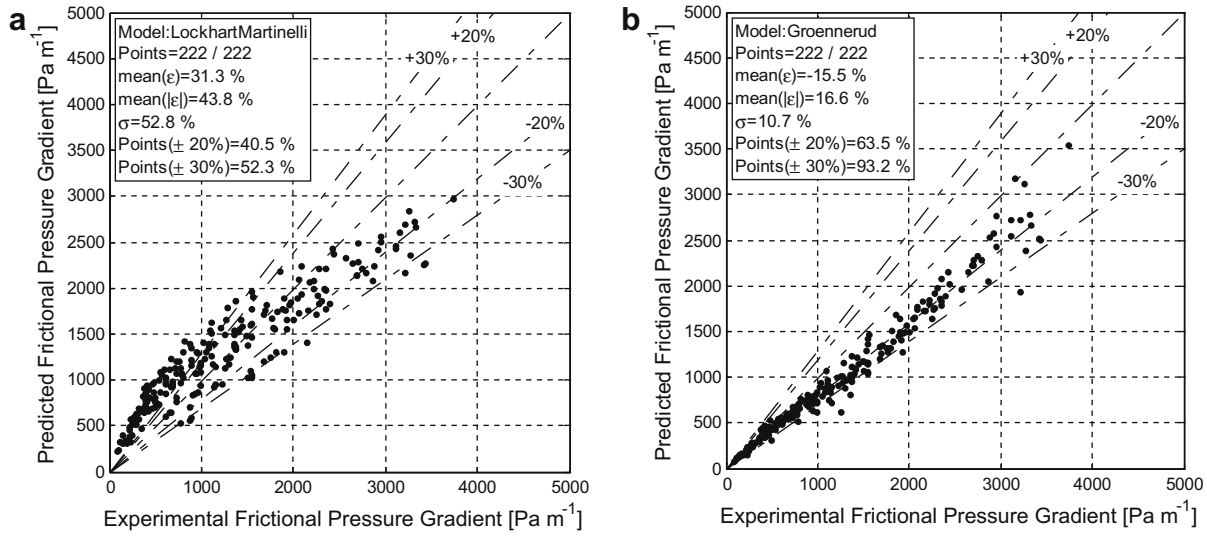


**Fig. 12.** Comparison of the experimental data to the predicted results of the models of (a) Lockhart and Martinelli [3] and (b) Grönnerud [5].

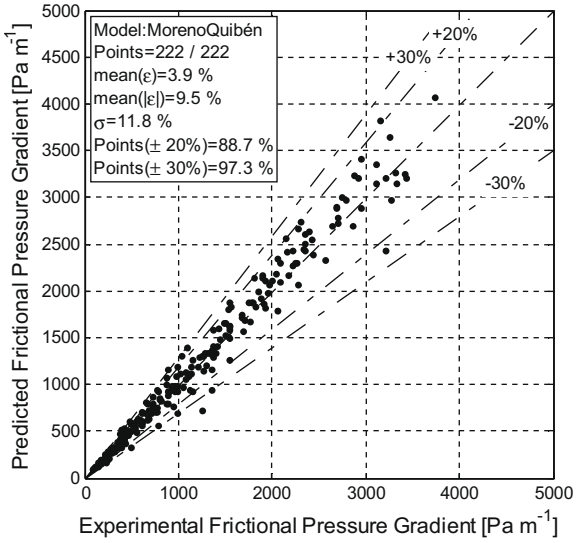


**Fig. 13.** Comparison of the experimental data to the predicted results of the model of Moreno Quibén and Thome [6].

### 7.3. Discussion

Fig. 14 depicts a final comparison between the experimental data (diabatic and adiabatic) and the cited prediction methods for two experimental conditions (a) $T_{sat} = -6.8$ °C, $G = 75$ kg s$^{-1}$ m$^{-2}$ and $q = 22.7$ kW m$^{-2}$ and (b) $T_{sat} = 6.1$ °C, $G = 125$ kg s$^{-1}$ m$^{-2}$ and $q = 23.0$ kW m$^{-2}$. These confirm the results shown in the previous paragraphs. The predictions from the model of Moreno Quibén and Thome follow the slope in the data very well, better than that of Grönnerud. The predictions of the models of Lockhart and Martinelli, Friedel and Müller-Steinhagen and Heck underpredict higher values of pressure drop (at higher vapor qualities) and overpredict lower values of pressure drop (at lower vapor qualities).

Table 4 shows the results segregated by flow pattern for both diabatic and adiabatic conditions. In terms of overall results, it can be seen that the model of Moreno Quibén and Thome is the one that predicts the experimental data the best, not only from the number of experimental data inside the error windows of ±20% and ±30% error, but also in terms of absolute mean error. Its values of mean error and standard deviation for both adiabatic conditions and overall data are close to the values obtained with the correlations of Müller-Steinhagen and Heck [4] and Grönnerud [5] which provide, respectively, the best results for these statistical variables.

For *stratified-wavy* flow, which represents almost 35% of the database, the best prediction statistics are obtained with the method of Moreno Quibén and Thome. The lower values of standard deviation are obtained with the correlation of Grönnerud, but this is similar to that obtained with the method of Moreno Quibén and Thome.

For *slug-strafied-wavy* flow, which represents less than 20% of the database, the best prediction statistics are obtained with the correlation of Grönnerud. In particular it predicts 100% of the diabatic data within ±30% error.

For *slug* flow, which represents less than 5% of the database, the best prediction statistics are obtained with the model of Moreno Quibén and Thome although the correlation of Grönnerud performs almost as well. In particular, both predict 100% of the diabatic data within ±20% error. The same applies for *intermittent* flow, representing less than 3% of the database, although the model of Friedel predicts 100% of the overall data within ±30% error.

Finally, for *annular* flow which represents about 38% of the database, the best prediction statistics are obtained with the model of Moreno Quibén and Thome, except for the standard deviation values, that are lower for the model of Grönnerud. In particular, the model of Moreno Quibén and Thome predicts 100% of the overall data within ±30% error.

It is surprising to observe the accuracy of the correlation of Grönnerud and of the phenomenological model of Moreno Quibén and Thome when considering that neither of these was developed or optimized for ammonia. Furthermore, it is also noteworthy that the correlations of Friedel and of Müller-Steinhagen and Heck produce a higher level of accuracy with this set of experimental data than what was observed by Thome et al. [9] with the data of Shah and Kabelac and De Buhr. Therefore, this raises several questions.

In Thome et al. [9] it was observed that the level of accuracy of the Moreno Quibén and Thome model was only 17% for predicting the experimental data of Kabelac and De Buhr and 56% for predicting the data of Shah. In the comparison it is clear that the Moreno Quibén and Thome model tends to underpredict the data of Shah and to overpredict that of Kabelac and De Buhr. Indeed, the data of Shah included a mixture of oil and ammonia (unspecified frac-

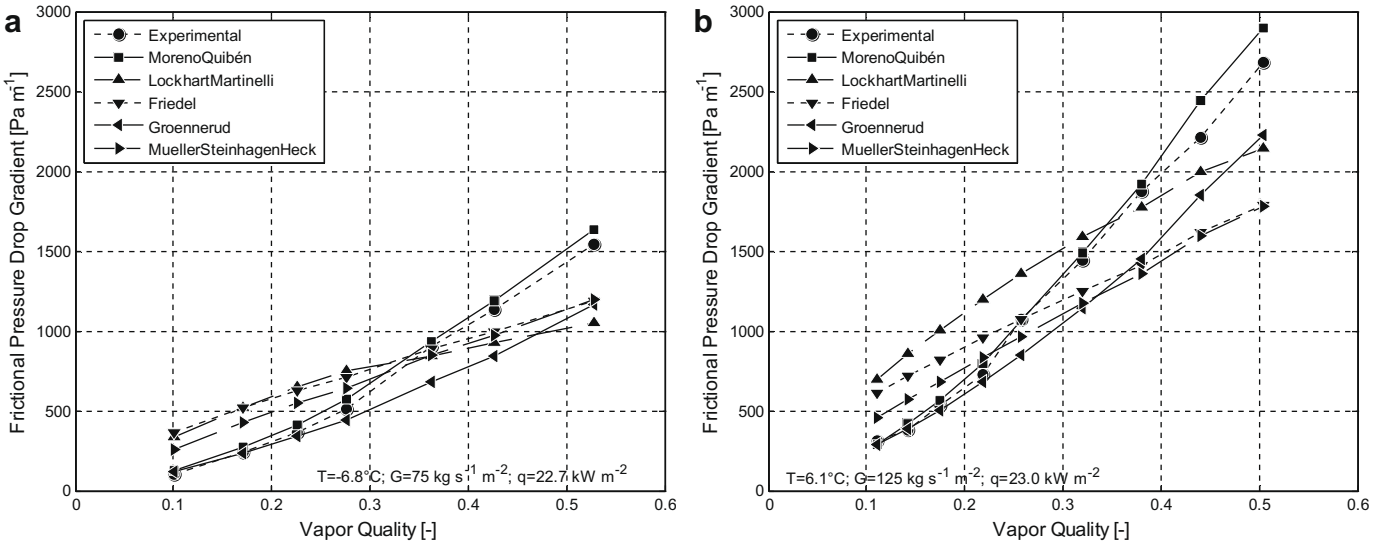


**Fig. 14.** Experimental diabatic and adiabatic data, and respective predicted data obtained with the cited methods for (a) $T_{sat} = -6.8$ °C, $G = 75$ kg s$^{-1}$ m$^{-2}$ and $q = 22.7$ kW m$^{-2}$; and (b) $T_{sat} = 6.1$ °C, $G = 125$ kg s$^{-1}$ m$^{-2}$ and $q = 23.0$ kW m$^{-2}$.

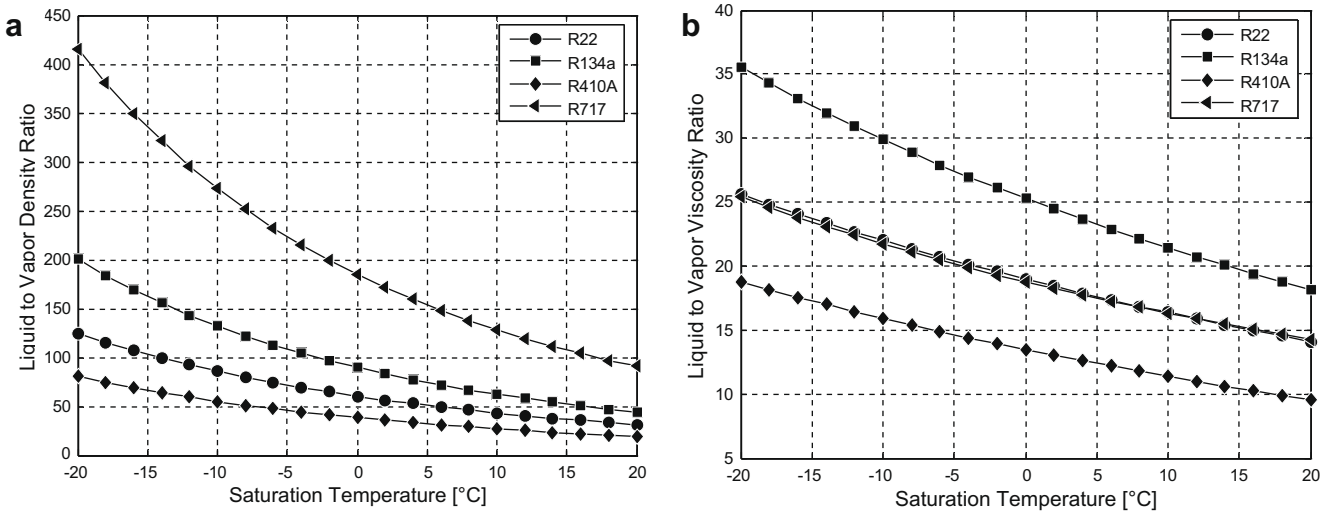


**Fig. 15.** Liquid to vapor physical properties ratios versus the saturation temperature for R22, R134a, R410A and R717 (ammonia): (a) density and (b) viscosity.

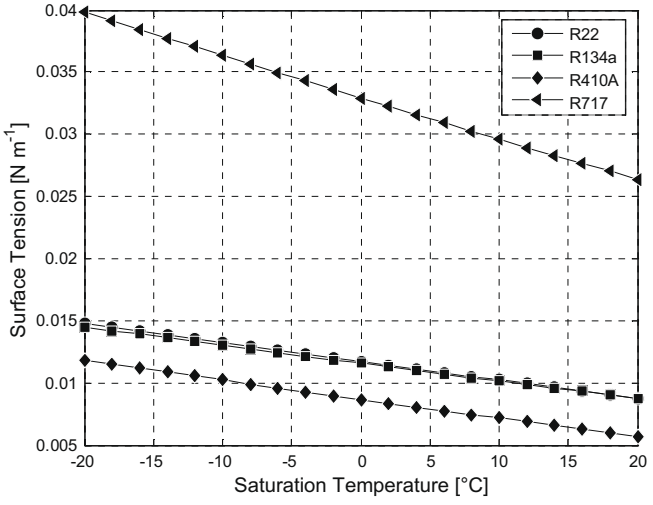


**Fig. 16.** Surface tension versus the saturation temperature for R22, R134a, R410A and R717 (ammonia).

tions), which would tend to increase the pressure drop, and thus could explain the underprediction of the data. It is still not clear why the model overpredicts the data for the smaller diameter (10.0 mm) tube of Kabelac and De Buhr.

As a final note, Fig. 15 compares the liquid to vapor (a) density and (b) viscosity ratios of ammonia to those of halocarbon refrigerants (R22, R134a and R410A) and Fig. 16 compares the surface tension of the cited refrigerants. As can be seen, apart from the viscosity ratio, the differences between ammonia and the cited halocarbon refrigerants are substantial. The difference in physical properties is less at higher saturation temperature and this may imply a better correspondence between experimental data and predictions. However, at present, validation of this point requires further experimental data and investigation.

## 8. Conclusions

This study presents new flow pattern observations and frictional pressure drop experimental data for ammonia. The number of pressure drop data is 124 under adiabatic and 98 under diabatic

conditions. Due to the range of experimental conditions, it gives an interesting insight and overview of the frictional pressure drop phenomena and provides a working base for both application and research engineers.

The flow patterns observed during the study included: *stratified-wavy*, *slug-stratified-wavy*, *slug*, *intermittent* and *annular*. These flow pattern observations were compared to the predictions of the flow pattern model of Wojtan et al. [1]. Three cases were studied (low, medium and high mass velocity) and flow patterns from both matched the predicted flow regimes, except for three vapor qualities near the intersection of two boundaries. This is because transitions are not line-wise but band-wise: the transition does not occur at one vapor quality but extends to a range of vapor qualities, until a particular flow pattern is fully established.

The experimental results show the traditional trend in the two-phase frictional pressure drop: it increases with mass velocity and vapor quality. Furthermore, it shows that diabatic and adiabatic pressure drops are similar, proving that there is not noticeable effect of the boiling process itself on the ensuing pressure gradient besides that of the acceleration of the flow, which is captured by the momentum pressure gradient.

The comparison of the experimental data against several existing methods shows that general empirical correlations tend to have poor levels of accuracy, as the number of predicted data does not exceeds 60% inside an error boundary of ±30%. An exception is the correlation of Grönnerud [5] which predicts 93% of the experimental data inside this error boundary. In the phenomenological category, the model of Moreno Quibén and Thome [6] has proved to be very accurate. It provides the best overall prediction results, with more than 97% of the experimental data predicted within ±30% error and almost 89% within ±20% error. The main prediction errors obtained with this model occur for the lowest pressure drops (those of the same order of magnitude as the uncertainty of the pressure transducer), which emphasizes its prediction accuracy.

For the particular set of conditions of this study, the authors recommend the use of the model of Moreno Quibén and Thome [6], rather than the correlation of Grönnerud [5]. Although more complicated to implement, the model from Moreno Quibén and Thome is preferred as it implies the use of flow pattern model of Wojtan et al. [1], thereby providing the influence of flow pattern on the process.

## Acknowledgements

The authors gratefully acknowledge the support of the EFROST (Efficient Food Storage) European Project under the Contract No. COOP-CT-2004-513106.

## References

[1] L. Wojtan, T. Ursenbacher, J.R. Thome, Investigation of flow boiling in horizontal tubes: part I – a new diabatic two-phase flow pattern map, Int. J. Heat Mass Transfer 48 (2005) 2955–2969.
[2] L. Friedel, Improved friction drop correlations for horizontal and vertical two-phase pipe flow, in: European Two-Phase Flow Group Meeting, paper E2, Ispra, Italy, 1979.
[3] R.W. Lockhart, R.C. Martinelli, Proposed correlation of data for isothermal two-phase two-component in pipes, Chem. Eng. Process 45 (1949) 39–48.
[4] H. Müller-Steinhagen, K. Heck, A simple friction pressure correlation for two-phase flow in pipes, Chem. Eng. Process 20 (1986) 297–308.
[5] R. Grönnerud, Investigation of liquid hold-up, flow-resistance and heat transfer in circulation type of evaporators, part iv: two-phase flow resistance in boiling refrigerants, in: Annexe 1972-1, Bull. de l'Inst. Froid, 1979.
[6] J. Moreno Quibén, J.R. Thome, Flow pattern based two-phase frictional pressure drop model for horizontal tubes. Part II: new phenomenological model, Int. J. Heat Fluid Flow 28 (2007) 1060–1072.
[7] G. Lorentzen, Ammonia: an excellent alternative, Int. J. Refrigeration 11 (1988) 248–252.
[8] O. Baker, Design of pipe lines for simultaneous flow of oil and gas, Oil Gas J. 53 (1954) 185–190.
[9] N. Kattan, J.R. Thome, D. Favrat, Flow boiling in horizontal tubes. Part 3: development of a new heat transfer model based on flow patterns, Heat Transfer 120 (1) (1998) 156–165.
[10] R.J. Silva Lima, J. Moreno Quibén, J.R. Thome, Flow boiling in horizontal smooth tubes: new heat transfer results for R-134a at three saturation temperatures, Appl. Therm. Eng. (2008), doi:10.1016/j.applthermaleng.2008.06.021.
[11] J.R. Thome, L. Cheng, G. Ribastki, L.F. Vales, Flow boiling of ammonia and hydrocarbons: a state-of-the-art review, Int. J. Refrigeration 31 (2008) 603–620.
[12] M.M. Shah, Heat transfer and pressure drop in ammonia evaporators, ASHRAE Trans. 80 (2) (1974) 238–254.
[13] M.M. Shah, Visual observations in an ammonia evaporator, ASHRAE Trans. 81 (1) (1975) 295–306.
[14] M.M. Shah, Heat transfer, pressure drop, visual observation, test data for ammonia evaporation inside pipes, ASHRAE Trans. 84 (1978) 238–254.
[15] S. Kabelac, H.-J. De Buhr, Flow boiling of ammonia in a plain and a low finned horizontal tube, Int. J. Refrigeration 24 (2001) 41–50.
[16] O. Zürcher, D. Favrat, J.R. Thome, Development of a diabatic two-phase flow pattern map for horizontal flow boiling, Heat Mass Transfer 45 (2002) 291–303.
[17] Refprop, Refrigerant Properties Database 23, Version 6.01. NIST, Gaithersburg, MD, 1998.
[18] Z. Rouhani, Modified correlations for void fraction and two-phase pressure drop, AB Atomernergi Sweden, AE-RTV-841, pp. 1–10, 1969.
[19] J.R. Taylor, An Introduction to Error Analysis, second ed., vol. 5, University Science Books, 1997.
[20] J.M. Mandhane, G.A. Gregory, K. Aziz, A flow pattern map for gas–liquid flow in horizontal pipes, Int. J. Multiphase Flow (1974) 537–553.
[21] Y. Taitel, A.E. Dukler, A model for predicting flow regime transitions in horizontal and near horizontal gas–liquid flow, AIChE J. 22 (2) (1976) 43–55.
[22] K. Hashizume, Flow pattern and void fraction of refrigerant two-phase flow in a horizontal pipe, Bull. JSME 26 (219) (1983) 1597–1602.
[23] N. Kattan, J.R. Thome, D. Favrat, Flow boiling in horizontal tubes. Part 1: development of a diabatic two-phase flow pattern map, Heat Transfer 120 (1998) 140–147.
[24] N. Kattan, J.R. Thome, D. Favrat, Flow boiling in horizontal tubes. Part 2: new heat transfer data for five refrigerants, Heat Transfer 1 (1998) 148–155.
[25] D. Steiner, Heat transfer to boiling saturated liquids, VDI-Wärmeatlas (VDI Heat Atlas), Verein Deutscher Ingenieure (VDI), Gessellschaft Verfahrenstechnik und Chemieingenieurwesen (GCV), in: J.W. Fullarton (Ed.), trans., Düsseldorf, 1993.
[26] J.R. Thome, J. El Hajal, Two-phase flow pattern map for evaporation in horizontal tubes: latest version, Heat Transfer Eng. 24 (6) (2003) 3–10.
[27] L. Wojtan, T. Ursenbacher, J.R. Thome, Interfacial measurements in stratified types of flow, part II: measurements for R-22 and R-410A, Int. J. Multiphase Flow 30 (2) (2004) 125–137.
[28] T. Ursenbacher, L. Wojtan, J.R. Thome, Interfacial measurements in stratified types of flow, part I: new optical measurement technique and dry angle measurements, Multiphase Flow 30 (2) (2004) 107–124.
[29] L. Wojtan, T. Ursenbacher, J.R. Thome, Investigation of flow boiling in horizontal tubes: part II, development of a new heat transfer model for stratified-wavy, dryout and mist flow regimes, Heat Mass Transfer 48 (2005) 2970–2985.
[30] J.R. Thome, J. El Hajal, A. Cavallini, Condensation in horizontal tubes, part 2: new heat transfer model based on flow regimes, Int. J. Heat Mass Transfer 46 (18) (2003) 3365–3387.
[31] J. El Hajal, J.R. Thome, A. Cavallini, Condensation in horizontal tubes, part 1: two-phase flow pattern map, Int. J. Heat Mass Transfer 46 (18) (2003) 3349–3363.
[32] L. Cheng, G. Ribatski, J. Moreno Quiben, J.R. Thome, New prediction methods for CO2 evaporation inside tubes: part I – a two-phase flow pattern map and a flow pattern based phenomenological model for two-phase flow frictional pressure drops, Int. J. Heat Mass Transfer 51 (1–2) (2008) 111–124.
[33] L. Cheng, G. Ribatski, J.R. Thome, New prediction methods for CO2 evaporation inside tubes: part II – an updated general flow boiling heat transfer model based on flow patterns, Int. J. Heat Mass Transfer 51 (1–2) (2008) 125–135.
[34] S.G. Bankoff, A variable density single-fluid model two-phase flow with particular reference to steam–water, J. Heat Transfer 11 (Series B) (1960) 265–272.
[35] A. Cicchitti, C. Lombardi, M. Silvestri, R. Soldaini, G. Zavattarelli, Two-phase cooling experiments – pressure drop, heat transfer and burnout measurements, Energia Nucleare 7 (6) (1960) 407–425.
[36] J.R.S. Thom, Prediction of pressure drop during forced circulation boiling of water, Int. J. Heat Mass Transfer 7 (1964) 709–724.
[37] B. Pierre, Flow resistance with boiling refrigerants – part 1, ASHRAE J. 6 (9) (1964) 58–65.
[38] C.J. Baroczy, A systematic correlation for two-phase pressure drop, Chem. Eng. Prog. Symp. Ser. 62 (44) (1965) 232–249.
[39] J.M. Chawla, Wärmeübergang und Druckabfall in waagerechten Rohren bei der Strömung von verdampfenden Kältemitteln, Chapter Lg1–Lg2. 523. VDI-Forschungsh, 1967.
[40] D. Chisholm, Pressure gradients due to friction during the flow of evaporating two-phase mixtures in smooth tubes and channels, Int. J. Heat Mass Transfer 16 (1973) 347–358.

[41] M.B. Ould Didi, N. Kattan, J.R. Thome, Prediction of two-phase pressure gradients of refrigerants in horizontal tubes, Int. J. Refrigeration 25 (2002) 935–947.
[42] J. Moreno Quibén, J.R. Thome, Flow pattern based two-phase frictional pressure drop model for horizontal tubes. Part I: diabatic and adiabatic experimental study, Int. J. Heat Fluid Flow 28 (2007) 1049–1059.
[43] N.P. Cheremisinoff, E.J. Davis, Stratified turbulent–turbulent gas–liquid flow, AIChE J. 25 (1979) 48–56.
[44] J.J.J. Chen, P.L. Spedding, An extension of the Lockhart–Martinelli theory of two-phase pressure drop and holdup, Int. J. Multiphase Flow 7 (1981) 659–675.
[45] V. Kadambi, Void fraction and pressure drop in two-phase stratified flow, Can. J. Chem. Eng. 59 (1981) 584–589.
[46] A.E. Dukler, M.G. Hubbard, A model for gas–liquid slug flow in horizontal and near-horizontal tubes, Ind. Eng. Chem. Fundam. 14 (1975) 337–347.
[47] E. Kordbyan, Some details of developing slugs in horizontal two-phase flow, AIChE J. 31 (1985) 802–806.
[48] C.J. Hoogendoorn, The characteristics of annular-mist flow in horizontal pipes, Symp. Two-phase Flow, Exeter, Devon, Paper (1965) C3.
[49] G.B. Wallis, Annular two-phase flow, part I: a simple theory, Trans. ASME J. Basic Eng. (1970) 59–72.
[50] K. Hashizume, Flow pattern, void fraction and pressure drop of refrigerant two-phase flow in a horizontal pipe II. Analysis of pressure drop, Int. J. Multiphase Flow 11 (1985) 643–658.
[51] J. Hart, P.J. Hamersma, J.M.H. Fortuin, Correlations predicting frictional pressure drop and liquid holdup during horizontal gas–liquid pipe flow with a small liquid holdup, Int. J. Multiphase Flow 15 (6) (1989) 947–964.